Assessing Hydrological Impacts of Deforestation and Land Use Change in the Tel River Basin

Triparna Sett[1*], Bhaskar R. Nikam[2], Vaibhav Garg[1], Praveen K. Thakur[1], Hukum Singh[3]
[1]Water Resources Department, Indian Institute of Remote Sensing, ISRO, Dehradun, India
[2]EDPO, Indian Space Research Organization Headquarters, Bengaluru, India
[3]Forest Research Institute, Dehradun, India
*Corresponding Author email: triparna35@gmail.com

(Received on 23 June 2026; In final form on 10 August 2026)

DOI: *https://doi.org/10.58825/jog.2026.20.2.346*

Abstract: Land use and land cover changes (LULCC) alter catchment hydrology by changing how water moves between the land surface and the atmosphere. This study examines how land use change between 1985 and 2015 affected the water balance of the Tel River basin, a sub-basin of the Mahanadi system in eastern India. Land cover maps for 1985, 1995, and 2005 were obtained from the national decadal LULC database, and a 2015 map was prepared from Landsat 8 imagery using a Random Forest classifier on Google Earth Engine (GEE) and later validated against NRSC data. The 2015 map reached an overall accuracy of 78.6 % (Kappa 0.68) against independent reference data. Forest and agriculture were mapped reliably, while the smaller classes of built-up land, bare land, and water body were combined into one less reliable category. Hydrological response was simulated with the Variable Infiltration Capacity (VIC) model for 1980 to 2018, using a one-factor-at-a-time design that holds climate constant so that only land use varies. Forest cover fell by 13.02% over the period, with most of the loss going to agriculture (about 1575 km^2). With climate held fixed, lower evapotranspiration (about 16 mm/year, or 1.7%) was passed almost entirely into higher surface runoff (about 7 mm, 2.0%) and higher base flow (about 9 mm, 4.6%), while long-term soil water storage stayed essentially unchanged. A pixel-level analysis shows that runoff rises in some parts of the basin and falls in others, so the basin average understates the local change in flood and erosion risk. The results point to the value of catchment-scale water management that accounts for where land use is changing within the basin.

Keywords: Land Use Land Cover Change (LULCC), Deforestation, Hydrological Modelling, Variable Infiltration Capacity (VIC) Model, Water Balance, Tel River Basin.

1. Introduction

The interaction between the Earth's surface and atmosphere is significantly altered by LULCC, which is widely acknowledged as a major driver of environmental change (Gashaw et al., 2018). Human activities remain the primary cause of these changes, according to subsequent research (Garg et al., 2019; Naha et al., 2021). LULCC significantly affects hydrological system efficiency and watershed dynamics. The impact of these variations on hydrological processes at the catchment scale is evaluated by changes in ET, surface runoff, groundwater recharge, water quality, baseflow, percolation, interaction, and sediment transport. Various studies have examined the hydrological effects of LULCC, especially in relation to deforestation (Garg et al., 2017; Berihun et al., 2019; Ghimire et al., 2021; Sulamo et al., 2021). Deforestation increases surface discharge, produces sediment, and degrades water quality, according to these studies. The hydrological balance has been altered due to simultaneously decreasing groundwater recharge and ET. To understand such intricate relationships, robust hydrological modelling techniques are necessary. The VIC model, a grid-based, semi-distributed land surface model developed by Liang et al. (1994, 1996) and Cherkauer et al. (2003), is ideal for simulating basin-scale dynamics using the coupled water and energy balance equations. The VIC model has been widely used in hydrological research across various climatic and geographic regions because of its proven ability to accurately simulate streamflow dynamics and systematically represent the water balance (Abdulla et al., 1996; Shrestha et al., 2012; Tavakoly et al., 2017; Zamani Sabzi et al., 2019; Niemeyer et al., 2018). The VIC model has also proven to be a useful tool for analysing the combined effects of climatic variability and LULCC on basin-scale hydrology across the Indian subcontinent. It has been used in many studies to investigate how changes in LULC and climate conditions affect soil moisture dynamics, ET, and runoff generation (Dadhwal et al., 2010; Nikam et al., 2018; Patidar and Behera, 2019; Hengade and Eldho, 2019; Kumari et al., 2021). The Tel watershed, a sub-basin of India's Mahanadi River system, has shown a growing susceptibility to extreme hydrological events, such as flash floods and extended droughts (Verma et al., 2022). Prior research in the field has mostly concentrated on features such as geomorphological evaluation (Verma et al., 2022), flood frequency estimation (Guru & Jha, 2015), and drought characterisation (Mishra & Nagarajan, 2011). However, only a few studies have looked at watershed processes across the Mahanadi basin using semi-distributed hydrological models and GIS tools (Dadhwal et al., 2010; Behera et al., 2018; Naha et al., 2021). To address this research gap, the current study undertakes a thorough

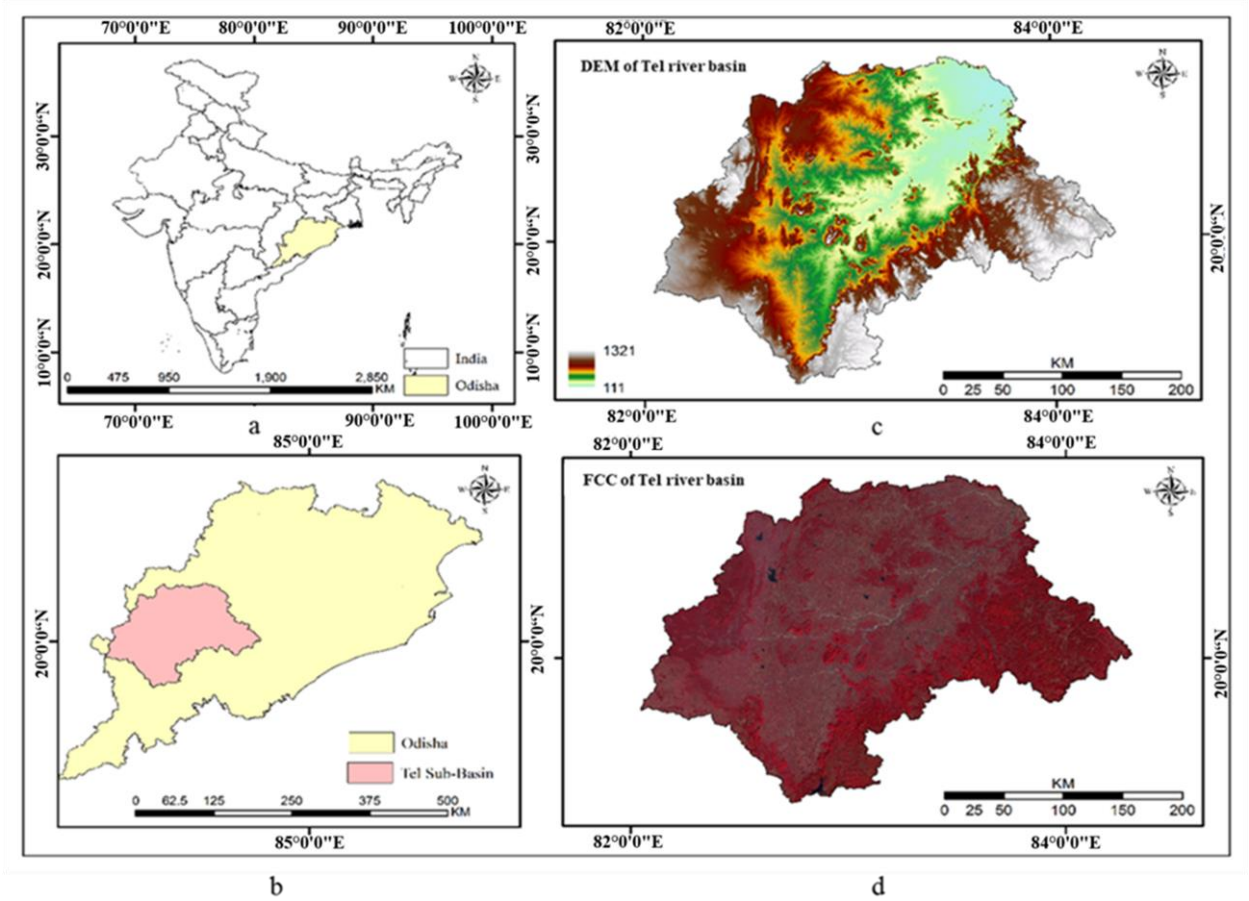


Figure 1: a) Odisha's location within India; b)spatial extent of the Tel river basin in Odisha; c)Digital Elevation Model of the Tel river basin; d) The FCC image of the Tel river basin derived from Landsat-8 OLI (Data acquisition date-01/10/2015-30/12/2015)

assessment of long-term hydrological dynamics in the Tel River basin from 1981 to 2018 at a spatial resolution of 5 km. This study aims to make three contributions: it separates the effect of land use from climate using a controlled one-factor-at-a-time design; it reports the hydrological response at the level of individual grid cells rather than only as a basin average; and it focuses on the dominant and reliably mapped forest-to-agriculture transition rather than on small, uncertain classes. The analysis evaluates the hydrological effects of widespread deforestation. The study's specific objectives are to: (1) use machine learning (ML) techniques to identify and quantify changes in land use and land cover (LULC); and (2) investigate how these changes affect critical hydrological components in the basin.

2. Methodology and Materials

2.1 Study Region

The Tel River, a major tributary of the Mahanadi River system, is located between 82°03' E and 84°17' E longitude, and 19°15' N and 20°55' N latitude. It is an essential component of the Mahanadi River basin's hydrological system. The watershed spans nearly 22,818 km² and is monitored by two primary gauging stations. The Kesinga station represents a catchment area of approximately 11,960 km², whereas the Kantamal station covers a significantly larger upstream catchment area of 19,600 km². The study region has a tropical climate with distinct dry and wet seasons, characterised by rainfall averages of 1360 mm and temperature ranges from 14°C to 42°C. The absence of the north-eastern monsoon results in a very harsh dry season from December to May. Rainfall variability leads to forest droughts and crop failures, underscoring the need to evaluate LULC changes in relation to basin hydrology.

The Tel River basin (Figure 1), an agriculture-dominated area, also contains several forest ecosystems, including tropical moist deciduous, tropical dry deciduous, semi-evergreen, and mangrove forests. Its spatially diversified land use pattern also includes grassland, shrubland, and plantations. Figure (1a to 1d) shows the geographical location of the Tel River basin in Odisha, along with elevation features, and a false colour composite (FCC) of the study area.

2.2 Quantifying the spatio-temporal LULC dynamics

LULC of the Tel River basin for 1985, 1995, and 2005 was extracted from decadal land-use/land-cover classification maps developed by Roy et al. (2015). For 2015, a high-resolution (30m) LULC map was prepared from Landsat-8 OLI images on Google Earth Engine (GEE). We evaluated Random Forest (RF) by Breiman (2001), Support Vector Machine (SVM) by Cortes and Vapnik

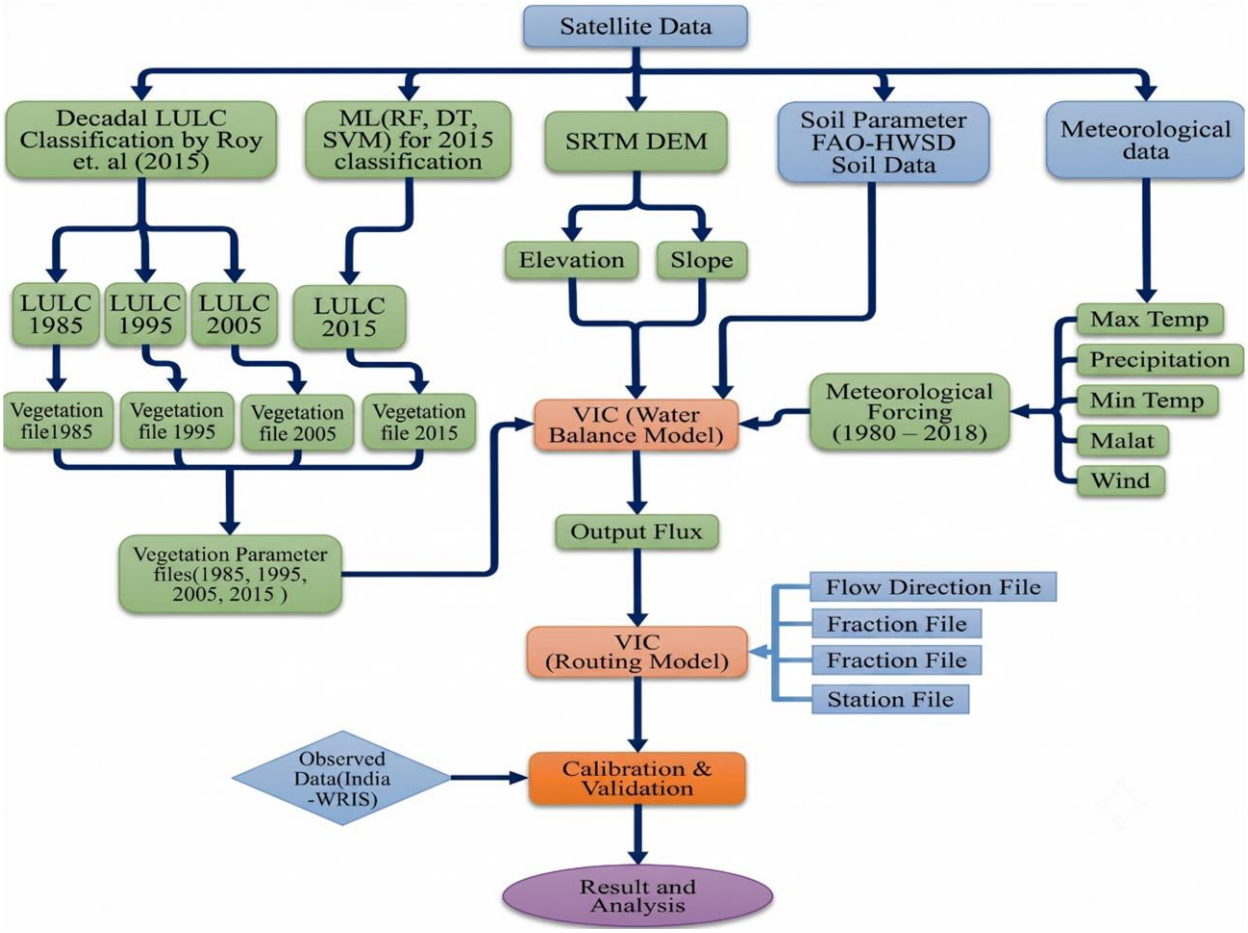


Figure 2: Flowchart showing the steps and variables involved in the methodology

(1995), and Quinlan's (1986) Decision Tree (DT), and compared the performance of non-parametric machine learning (ML) algorithms.

Due to their efficiency and precision, ML models are used for classification, and RF consistently emerges as the most accurate due to its superior handling of high-dimensional data and resistance to overfitting. The RF algorithm operates as an ensemble of randomized decision trees, where the final class prediction $\hat{C}(x)$ for an input feature vector x is the determined via majority voting.

$$\hat{C}(x) = mode\ \{h_k(x)\}_{k=1}^{K} \qquad \text{Eq. (1)}$$

Where $h_k(x)$ represents the k-th individual decision tree, and K represents the total number of trees in the ensemble. The predicted class for each pixel is the most frequent; this is the mode, taken over the set of K tree outputs.

Knowledge-based modifications are employed to enhance classification accuracy at various stages, thereby minimising spectral confusion. The accuracy of the LULC maps is evaluated using high-resolution remote sensing images from the NRSC for 2015. This machine learning approach, supplemented by iterative adjustments, demonstrates a robust methodology for precisely characterising the terrain over the period. The spatio-temporal LULC dynamics at the pixel level include precise measurements of changes in the Tel River basin. The ML-classified maps are standardised at a 100 m resolution. The 30m LULC (2015) was resampled to the 100 m grid using a nearest neighbour resampling filter, which preserves categorical class values and avoids introducing spurious change-detection artefacts along pixel boundaries.

The 2015 classifier was trained on labelled samples collected across the basin for each class, and its accuracy was assessed against an independent set of reference points. The limitation of this study is that the land cover maps come from two different sources. The maps for 1985, 1995, and 2005 are from the decadal national database, while the 2015 map was prepared here with a different classifier and class scheme. Comparing maps made by different methods can introduce apparent change that is really a classification difference rather than a real land cover change (Table 3). To put this in context, the cross-check of the 2015 map against independent reference data (NRSC) showed disagreement of about 22%, which is larger than the roughly 10% of land area that the national database reports as changing across India between 1985 and 2005. For this reason, the small area classes are treated as uncertain, and the main interpretation rests on the large and consistent forest-to-agriculture change, which is the dominant transition in the basin and is least sensitive to these differences.

2.3 VIC Model Simulation

The model integrates topographic, vegetation, and soil data to simulate hydrological processes. It is a grid-based model that utilises coupled water and energy balance

Table 1: Details of the datasets used for this study

Variable	Product	Resolution	Period	Source
LULC 1985, 1995, 2005	Decadal national LULC	100m	1985, 1995, 2005	Roy et al., 2015
LULC 2015	RF on Landsat 8 OLI (GEE)	30 m	2015	This study
Meteorological forcing	ERA5- Land	~9 km	1980 to 2018	Munoz-Sabater 2021
Soil	Harmonised World Soil Database v2.0	~1 km	Static	Nachtergaele et al., 2023
DEM	SRTM v3	30 m	Static	Farr et al., 2007
Leaf Area Index	MODIS MCD15A2	500 m	Monthly	MODIS
Discharge	India-WRIS, Kantamal station	Daily	1980 to 2018	India-WRIS

equations, making it robust for basin-scale hydrodynamics. Model inputs are generated using several parameter files, including the vegetation parameter file, vegetation library, soil parameter file, and meteorological forcing data (Table 1). Topographic inputs, including elevation, slope, and flow direction, were derived from the Shuttle Radar Topography Mission (SRTM) Version 3 Digital Elevation Model (DEM) at 30 m resolution (Farr et al., 2007).

To quantify hydrological impacts, the physically based, semi-distributed VIC model (VIC-3L, v4.2d) is configured to simulate the water balance mode on the Tel River basin. The model solves the water balance equation at each time step t for every grid cell as per the following equation.

$$\frac{\partial S}{\partial t} = P - E - R - B \qquad \text{Eq. (2)}$$

This is the primary water balance equation, where S is the soil moisture storage, P is precipitation, E is evapotranspiration, R is surface runoff, and B is baseflow. The overall methodological framework adopted in this study is illustrated in Figure 2.

Surface Runoff and Infiltration Capacity (Variable Infiltration Curve)

The model is discretised in water balance mode at a daily timescale with a spatial resolution of 0.05 ° × 0.05 °. The vertical soil column is divided into three layers. The upper two layers control rapid runoff via the variable infiltration capacity curve using the Xiangjiang formulation (Zhao, 1980), described by the infiltration capacity I relative to the maximum infiltration capacity.

$$i = i_m \left[1 - (1 - A)^{1/b_i}\right] \qquad \text{Eq. (3)}$$

Where i is the infiltration Capacity (mm/hr); i_m is the Maximum Infiltration capacity of the area related to the saturated hydraulic conductivity; A is the fraction of the grid cell saturated, and b_i is the infiltration shape parameter. This parameter defines the curvature of the infiltration curve, thereby governing the partition between infiltration and saturation excess overland flow.

A. Baseflow (Subsurface Runoff)

Baseflow generation from the third (deep) soil layer follows the Arno formulation (Franchini & Pacciani, 1991), which exhibits non-linear behaviour as the soil moisture approaches saturation:

$$R_b = \frac{D_{\max}\left[W_3/W_{s,3}\right]^2}{1 + D_{max}/W_{s,3}\left[W_3/W_{s,3}\right]^2} \qquad \text{Eq. (4)}$$

Where R_b is the baseflow rate, W_3 is the current soil moisture in the third layer, $W_{s,3}$ is the maximum soil moisture capacity of the third layer, and D_{max} is the maximum baseflow drainage rate occurring at the full saturation soil moisture capacity ($W_{s,3}$) where non-linear baseflow begins.

Table 2: Calibrated VIC soil parameters and their sensitivity ranges for the Tel River Basin

Parameter	Symbol	Calibrated value	Range tested
Infiltration shape parameter	b_i	0.4	0 to 0.4
Maximum baseflow fraction	D_s	0.001	0 to 1
Baseflow threshold (fraction of maximum soil moisture)	W_s	0.9	0 to 1
Top soil layer depth	d_1	0.9 m	0.1 to 1.5 m
Middle soil layer depth	d_2	1.0 m	0.1 to 1.5 m
Bottom soil layer depth	d_3	0.7 m	0.1 to 1.5 m

Table 3: Comparative Evaluation of ML techniques for LULC classification accuracy

ML Algorithm	Overall accuracy	Kappa coefficient
DT	74.01%	0.63
SVM	83.03%	0.74
RF	95.69%	0.85

B. Evapotranspiration

Total Evapotranspiration is the sum of the three components, calculated for each vegetation tile and then averaged over the grid cells

$$E = E_{canopy} + E_{transpiration} + E_{bare\ soil} \quad \text{Eq. (5)}$$

Each component is typically calculated using a variation of the Penman-Monteith equation to couple the water budgets. The Penman-Monteith Equation for the latent heat flux is as follows:

$$\lambda E = \frac{\Delta(R_n - G) + \rho_a c_p (e_s - e_a)/r_a}{\Delta + \gamma(1 + r_c/r_a)} \quad \text{Eq. (6)}$$

Where, λ is the latent heat of vaporization; R_n is net radiation; G is ground heat flux; Δ is the slope of the saturated vapour pressure curve; ρ_a is the density of air; c_p is the specific heat of air; e_s-e_a is a vapour pressure deficit; r_a is aerodynamic resistance; r_c is canopy resistance; γ is the psychrometric constant.

Leaf Area Index (LAI), albedo, and architectural resistance are parameters that influence vegetation dynamics, which in turn affect the Penman-Monteith calculation for evapotranspiration. The grid-based runoff and baseflow are routed to the basin outflow and estimated using a routing model that utilises a coupled linearized Saint-Venant equation (Lohmann et al., 1996) and an instantaneous unit hydrograph for in-grid and channel routing.

Meteorological forcing files (precipitation, maximum and minimum temperature, and wind speed) are obtained from the ERA-5 Land dataset (Muñoz-Sabater et al., 2021) at a resolution of 9 km. Soil hydraulic properties (porosity, saturated hydraulic conductivity K_{sat}, field capacity, and wilting point) are derived from the Harmonised World Soil Database (HWSD) (Nachtergaele et al., 2023) using pedotransfer functions (PTFs) from Cosby et al. (1984) and Reynolds et al. (2000).

$$\Psi = \mathrm{f}(\%\mathrm{Sand}, \%\mathrm{Clay}, \%\mathrm{Organic\ Matter}) \quad \text{Eq. (7)}$$

Where Ψ represents a soil hydraulic property (SHP) used by the VIC model (such as K_{sat}, porosity, or Field capacity); % Sand, % Clay, and % Organic Matter are the input variables-basic soil physical properties that are typically derived from soil maps (HWSD). The regression relations for porosity, saturated matric, the pore size index (b), and saturated hydraulic conductivity follow (Cosby et al., 1984), and the exact coefficients used are given with the equation.

Monthly LAI data derived from the MODIS LAI Product (MCD15A2) at 500 m resolution provided a monthly climatology for canopy resistance calculation along with vegetation phenology. Daily discharge data (1980-2018) from the Kantamal gauging station, acquired from the India WRIS portal, served as the benchmark for model calibration.

Surface runoff is simulated using the Xinanjiang formulation (Zhao, 1980) via infiltration through the upper two soil layers within the VIC framework. The Arno formulation (Franchini & Pacciani, 1991) controls baseflow generation from the third soil layer. The basin outflow is estimated using a routing model, which employs a coupled linearized Saint-Venant equation (Crompton, 2019) and an instantaneous unit hydrograph.

2.4 Parameterisation and Validation

The model is calibrated by optimisation of six sensitive soil parameters: the thickness of three soil layer depths (d_1, d_2, d_3), the infiltration shape parameter (b_i), which governs the distribution of precipitation between infiltration and direct runoff, the threshold for starting non-linear baseflow as a percentage of maximum subsurface flow (D_s), and the threshold for non-linear baseflow occurrence as a percentage of maximum soil moisture (W_s).

The infiltration shape parameter (b_i) is critical; a higher value of bi results in lower infiltration capacity across the grid cell, enhancing surface runoff generation. Similarly, soil depths regulate the total water-holding capacity, directly influencing evapotranspiration memory and baseflow recession. The parameters D_s and W_s define the recession curve; a lower D_s enhances baseflow during dry periods, while a higher W_s delays the onset of non-linear rapid baseflow drainage. The model performance is evaluated by the Nash-Sutcliffe Efficiency (NSE), defined as:

$$NSE = 1 - \frac{\sum_{t=1}^{T}(Q_{obs}^t - Q_{sim}^t)^2}{\sum_{t=1}^{T}(Q_{obs}^t - \bar{Q}_{obs})^2} \quad \text{Eq. (8)}$$

Where Q_{obs} and Q_{sim} are observed and simulated discharges, respectively. The VIC model, as a credible tool for hydrological dynamics assessment, is evaluated using the Nash-Sutcliffe Efficiency together with the percent bias (PBIAS) and the coefficient of determination (R^2), following the model performance ratings of (Moriasi et al., 2007).

A period of 1980-2018 is used for the simulation, and the model is validated using observed discharge data from the Kantamal gauging station. To maintain methodological rigor and address potential autocorrelation bias, the study is done using non-overlapping intervals: the calibration (1985-2005) and validation (2007-2018) periods. Table 2. Calibrated VIC soil parameters for the Tel basin and the ranges explored during calibration. These values are the selected parameter set from the calibration run.

2.5 Scenario-based assessment

A scenario-based assessment is performed using a "One Factor At a Time" (OFAT) simulation strategy to minimise the impacts of climate variability on LULC. Using LULC data from different years, a four-model simulation scenario (S1, S2, S3, S4) is created, keeping a constant

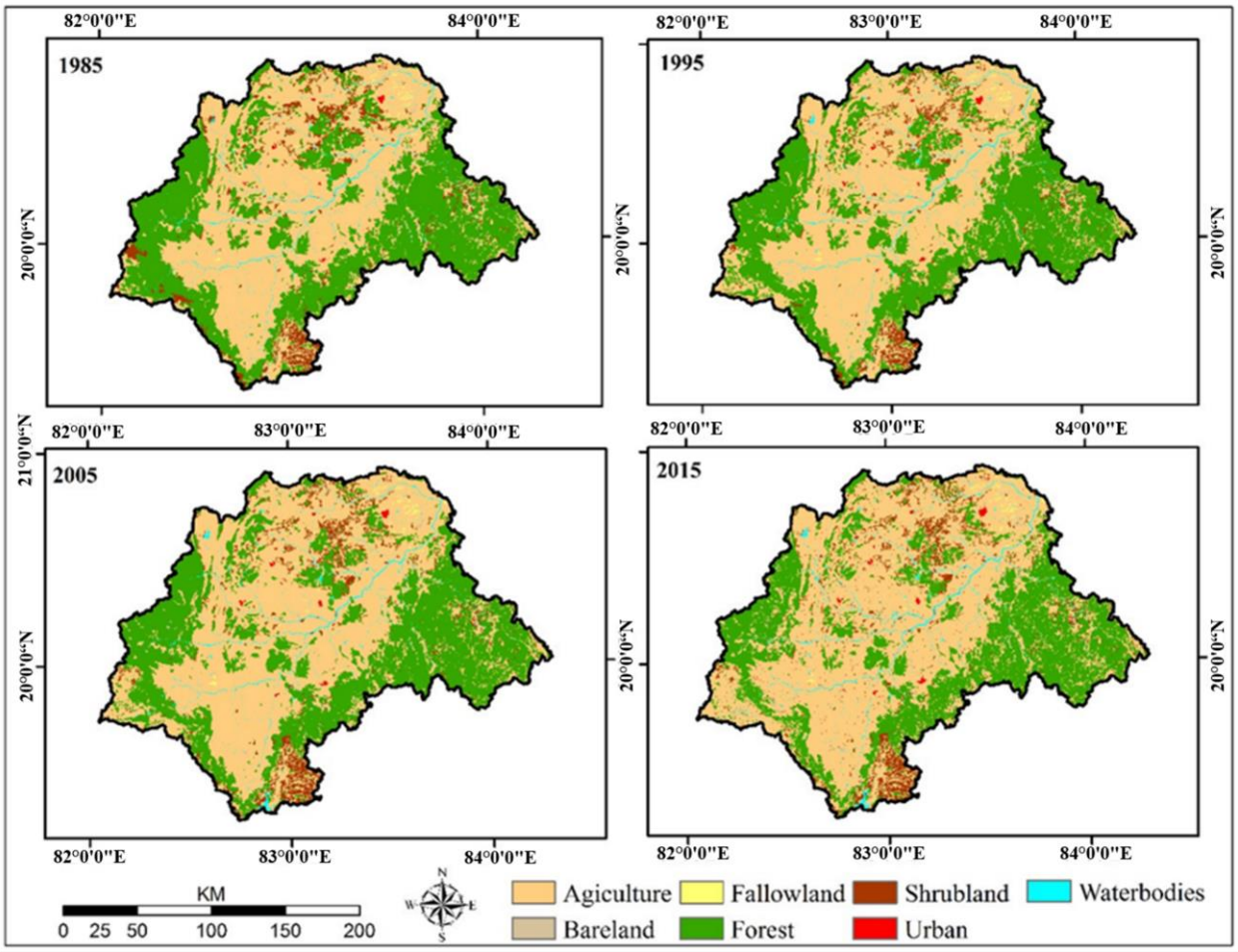


Figure 3: Spatiotemporal LULC mapping of the Tel river basin (1985, 1995, 2005, and 2015)

meteorological forcing M (t) dataset (1980-2018) and a static LULC map (1985, 1995, 2005, and 2015, respectively).

Mathematically, the hydrological response H for a scenario S_k using LULC map L_k is given by:

$$H(S_k) = f_{VIC}(LULC_k, M_{1980-2018}) \quad \text{Eq. (9)}$$

Where, $H(S_k)$ is the hydrological responses (total runoff, evapotranspiration, or streamflow, simulated for a specific scenario S_k); f_{VIC} represents the VIC Hydrological Model Function, which takes input data and simulates the water balance; $LULC_k$ is the Land Use Land Cover Map used for the specific scenario k (LULC from 1985, 1995, 2005 and 2015); $M_{(1980-2018)}$ is the meteorological forcing (eg: precipitation, temperature and wind speed) for the entire baseline period (1980-2018) which kept constant across all the scenarios.

$$\Delta H_{LULC} = H(S_k) - H(S_1) \quad \text{Eq. (10)}$$

Where ΔH_{LULC} is the anomaly in Hydrological Responses caused only by the LULC change between the baseline year and the scenario year k. $H(S_k)$ is the simulated hydrological response for scenario S_k, which uses the LULC map from a later decade (eg: 1995, 2005, and 2015); $H(S_1)$ is the simulated hydrological response for the baseline scenario (S1), which uses the earliest LULC map (1985 LULC) but the same constant meteorological forcing.

By subtracting the baseline response $H(S_1)$from the scenario responses $H(S_k)$, the long-term effect of the climate is effectively cancelled out, isolating the pure effect of the change in LULC (deforestation, urbanisation, etc.) on hydrological components like Evapotranspiration (ET), Runoff (R), and Baseflow (B).

This work provides a robust framework for identifying the impacts of LULC dynamics on basin-scale hydrology and offers actionable insights for sustainable watershed management. The calibration phase utilized data from 1985 to 2005, while validation was performed using data from 2007 to 2018.

3. Results and Discussion

Spatiotemporal Mapping and Analysis of LULC Dynamics

Among the three machine learning classifiers evaluated, the Random Forest (RF) model yielded the highest classification accuracy and Kappa coefficient, and was subsequently selected to generate the 2015 LULC map for the Tel River basin (22,818 km^2). To validate the final product, the RF-derived LULC map was separately cross-compared against independent NRSC-derived reference data. This external validation yielded an overall accuracy of 78.6% with a Kappa coefficient of 0.68. While agricultural and forest lands showed high agreement with the NRSC baseline, the merged built-up class exhibited

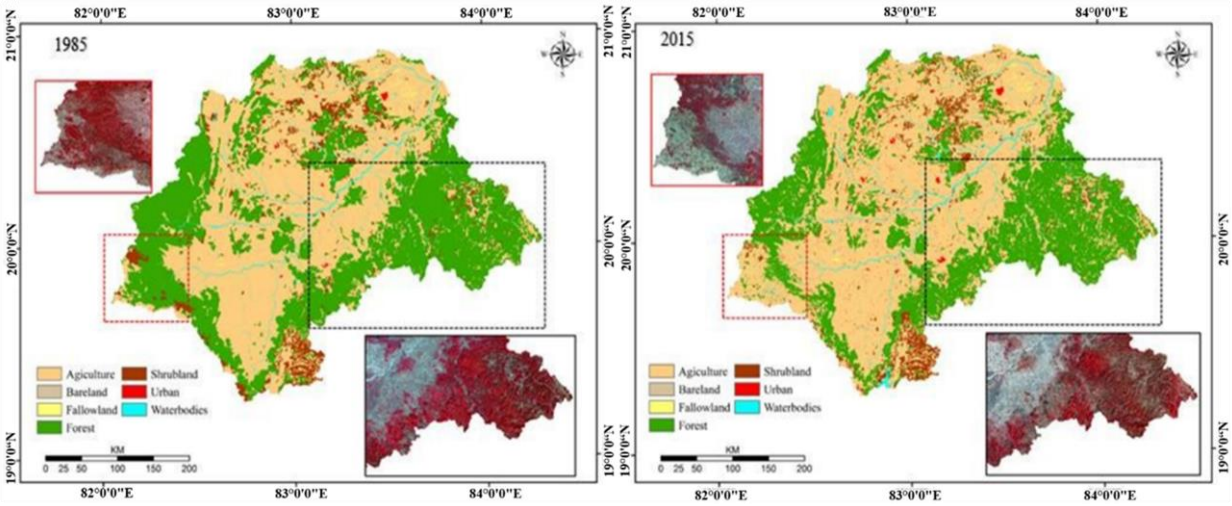


Figure 4: FCC Image and LULC Analysis of the Study Region: a) 1985; b) 2015

slight over-prediction. The initial 95.69% accuracy (kappa = 0.85) reported in Table 3 reflects the internal training and validation phase of the RF model. In contrast, the 78.6% figure represents its true spatial agreement when evaluated against the official NRSC dataset.

Two methods were used to evaluate the LULC dynamics: a) a class-wise LULC change compared to the 1985 baseline, and b) identifying spatial patterns of transformation at a finer (100m) spatial resolution. Figure 3 shows the spatiotemporal extent of the LULC classes across the study period.

The three-decade LULC dynamics across the Tel River basin (1985–2015) reveal substantial spatial transformations driven primarily by deforestation, agricultural intensification, and urban growth (Table 4, Table 5). Forest cover (F) experienced the largest absolute reduction, declining by 1,247.23 km^2 (-13.02%) from 9,581.46 km^2 to 8,334.23 km^2, with the bulk of cleared forest undergoing transition to agricultural land (1,575.43 km^2) and shrubland (265.99 km^2) (Table 4. & 5.). Driven predominantly by this forest conversion, agricultural land (AG) expanded by 1,077.88 km^2 (+9.50%), reaching a final area of 12,423.70 km^2 (Table 4, Table 5). Urban settlements (UR) recorded the highest relative growth rate, increasing by 136.68% (+64.05 km^2), primarily at the expense of pre-existing cropland (66.09 km^2) (Table 4, Table 5). Additionally, water bodies (WB) contracted by 100.42 km^2 (-22.54%), with 154.94 km^2 transitioning into agricultural use (Table 4, Table 5). Despite these active land transitions, agricultural land (10,473.02 km^2) and forest cover (7,701.10 km^2) demonstrated the highest overall spatial stability, as indicated by the diagonal values of the transition matrix (Table 4). Alongside, Table 6 outlines the conversion pathways of forest cover to other land use and land cover (LULC) classes over the 30-year study period (1985–2015)

Table 4: Changes Matrix of Decadal LULC (km^2) from 1985 to 2015

		LULC of 2015							
		AG	**BL**	**FL**	**F**	**SL**	**UR**	**WB**	**Total**
LULC of 1985	**AG**	***10473.02***	*1.27*	*6.77*	*265.65*	*467.56*	*66.09*	*65.46*	***11345.82***
	BL	*4.97*	***10.02***	*0*	*6.22*	*12.53*	*0*	*0.28*	***34.02***
	FL	*36.31*	*4.24*	***37.73***	*1.78*	*3.28*	*0.04*	*0.85*	***84.23***
	F	*1575.43*	*5.72*	*1.55*	***7701.1***	*265.99*	*8.13*	*23.54*	***9581.46***
	SL	*176.92*	*0.89*	*0.19*	*325.16*	***746.74***	*0.06*	*4.59*	***1254.55***
	UR	*2.11*	*0*	*0*	*8.22*	*0*	***36.5***	*0*	***46.83***
	WB	*154.94*	*0.17*	*0.13*	*26.1*	*13.74*	*0.06*	***250.3***	***445.44***
	Total	***12423.7***	***22.31***	***46.37***	***8334.23***	***1509.84***	***110.88***	***345.02***	***22792.35***

***The diagonal values for respective LULC classes are given in bold, indicating the area that has stayed unaltered between the two periods.*

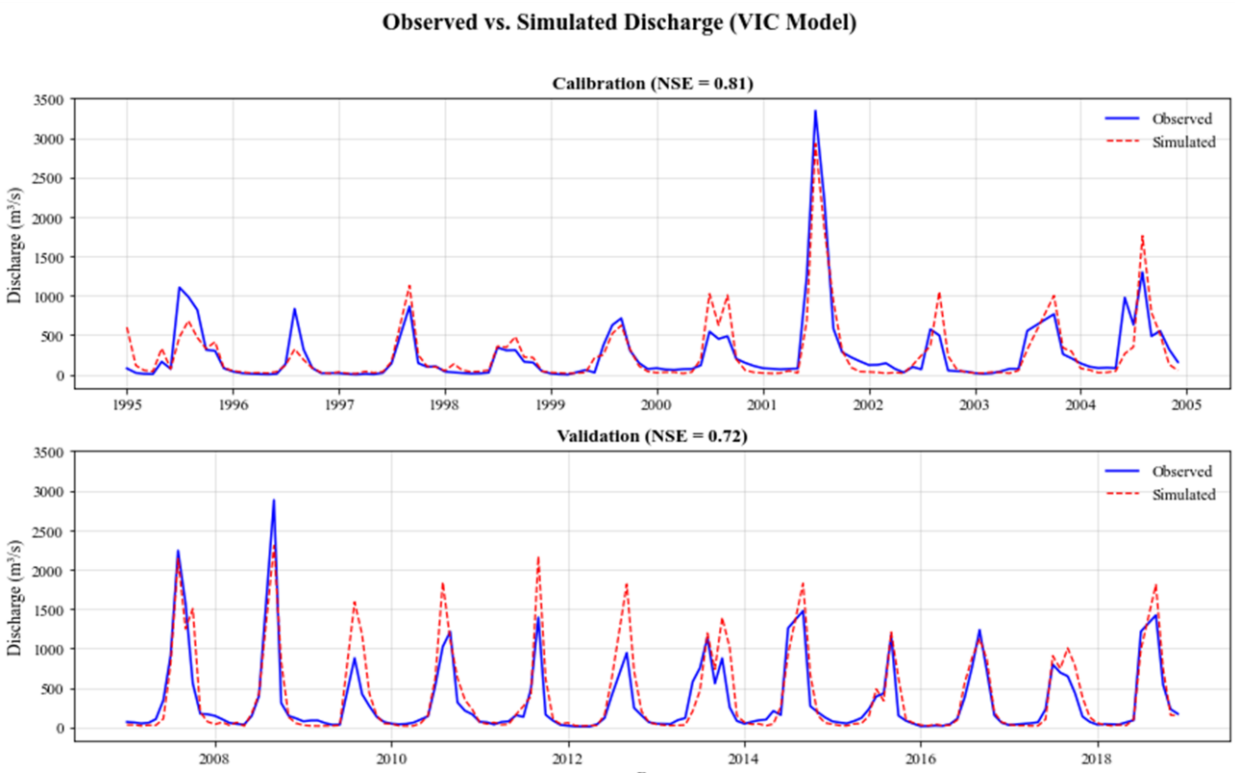


Figure 6: NSE Values during VIC Model Calibration and Validation

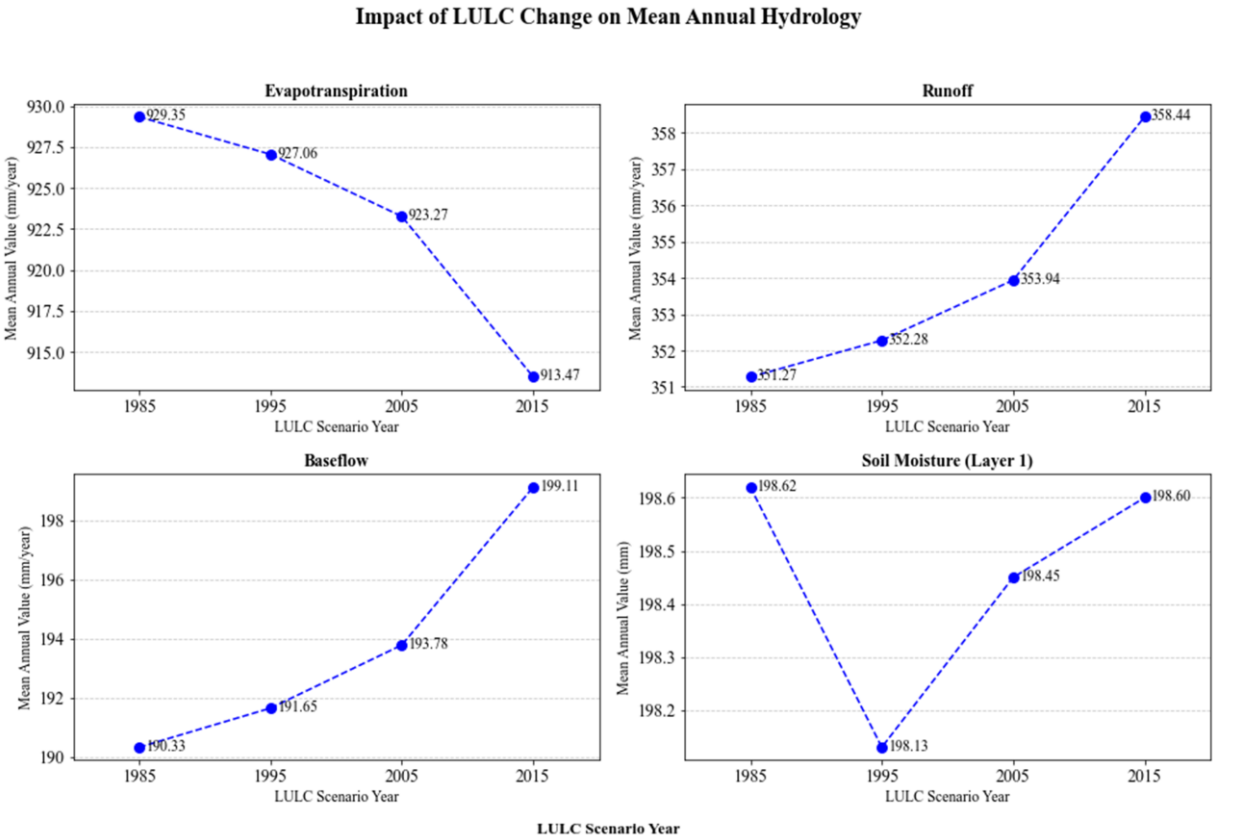


Figure 6: Trends in Hydrological Components across four LULC Scenarios in (A) Surface runoff; (B) Evapotranspiration; (C) Baseflow; (D) Soil Moisture (Layer 1)

By 2015, the overall boundaries of the forested region remained essentially unchanged in the eastern part (Figure 4b) of the basin; however, the density and quality (health) of the forest had drastically decreased due to logging, grazing, or other anthropogenic influences.

In comparison, the western part (Figure 4a) of the basin exhibits a significant decline in forest cover due to conversion to other land-use classes. To visualise the changes that happened between 1985 and 2015, a land

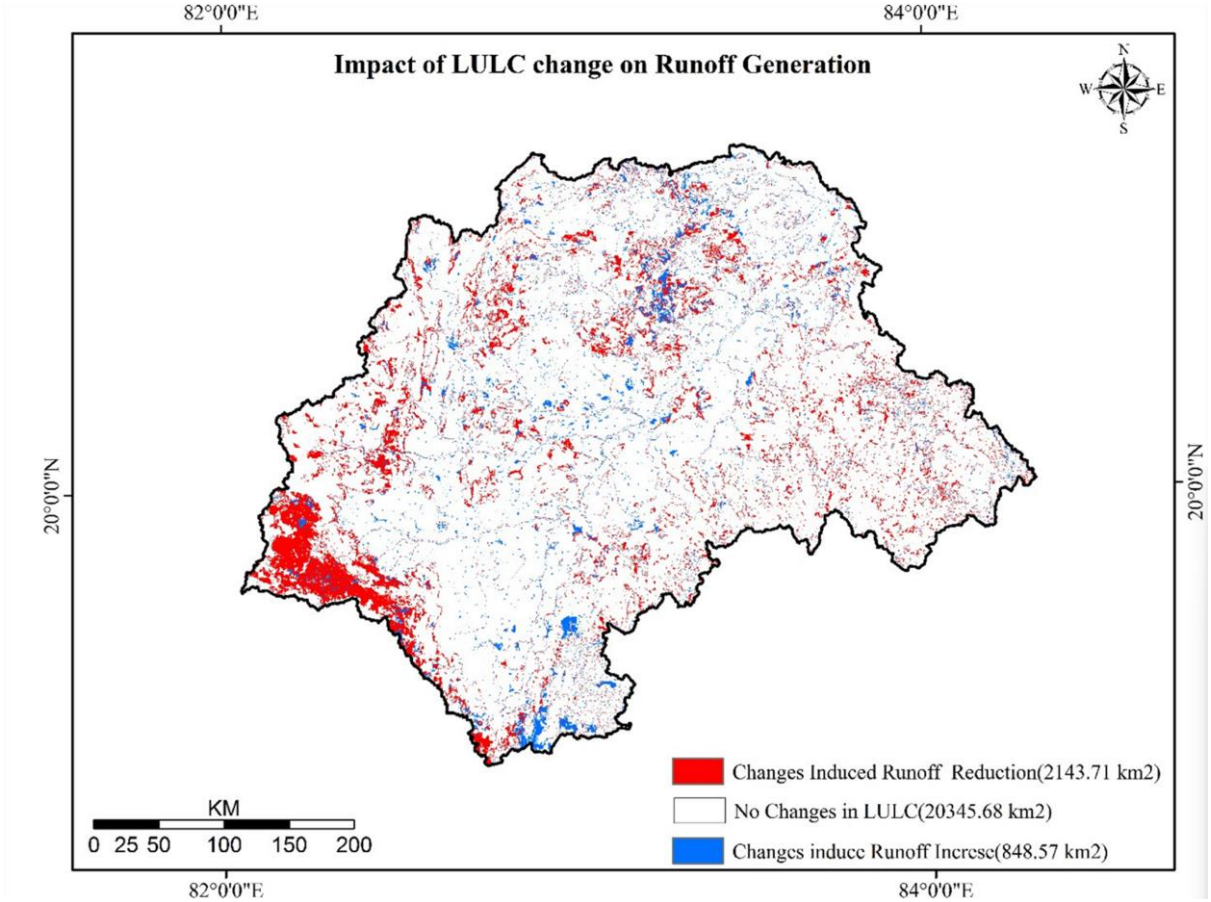


Figure 7: Runoff response to LULC Transformation

cover conversion map (Figure 7) is prepared to show landscape modifications over time.

VIC model simulation and performance

The VIC model is used to quantify the impacts of LULC change on hydrological components. By integrating satellite-derived vegetation datasets with in-situ soil and climatic data, the model simulates land surface processes. The calibration (1985-2005) and validation (2007-2018) periods were kept as non-overlapping intervals to address potential autocorrelation issues and to ensure methodological rigour. By achieving a Nash-Sutcliffe Efficiency (NSE) of 0.81 for calibration and 0.72 for validation models (Figure 5), the performance is robust, which falls within the 'good' performance range for the Nash-Sutcliffe Efficiency (ASCE, 1993)

Hydrological responses to LULCC

The scenario-based analysis (S1 to S4) confirmed the LULCC impacts on hydrological balance by demonstrating a consistent shift in the basin's hydrological components (Figure 6).

Surface Runoff

Mean annual surface runoff increased from 351.27 mm/yr (S1) to 358.44 mm/yr (S4), a total of 7.17 mm (2.04%) increase (Tables 7 & 8). The conversion of permeable forest and fallow lands into impervious urban areas and agricultural utilities is the leading cause. Impervious

Table 5: % of change in LULC (km2) during the year 1985 to 2015

LULC Class	Initial Area(km²) (1985)	Final Area(km²) (2015)	Net Change (km²)	Percentage Change (%)
AG	11,345.82	12,423.70	+1,077.88	+9.50%
BL	34.02	22.31	-11.71	-34.42%
FL	84.23	46.37	-37.86	-44.95%
F	9,581.46	8,334.23	-1,247.23	-13.02%
SL	1,254.55	1,509.84	+255.29	+20.35%
UR	46.83	110.88	+64.05	+136.68%
WB	445.44	345.02	-100.42	-22.54%

Table 6: Quantified changes of Forest to other Land Cover Categories (km²)

Conversion from Forest to other Land Cover	Area (km²)
Forest-Agriculture	1575.43
Forest-Bareland	5.72
Forest-Fallowland	1.55
Forest-Shrubland	265.99
Forest-Urban	8.13
Forest-Waterbodies	23.54
Total Area	1880.38

surfaces limit water percolation, increasing direct runoff, which amplifies the potential for flash floods and accelerated soil erosion, particularly in areas where protective vegetation cover is removed (Guru & Jha, 2015).

This direction of change agrees with the wider literature on deforestation and runoff. Forest soils usually have high infiltration capacity because of root channels, surface litter, and stable aggregates. So the loss of forest and the spread of cropland and built-up surfaces lowers infiltration and increases the share of rainfall that leaves as quick runoff. (Bruijnzeel, 2004; Bosch & Hewlett, 1982). The ~2% increase found here is smaller than values reported for basins with more complete clearing, for example, the runoff rise of roughly 9% reported for the Andassa watershed (Gashaw et al., 2018). The smaller response in the Tel basin reflects both the partial nature of the forest loss and opposing within-basin changes discussed in the following sections. The spatial pattern in Figure 7 gives this a direct management application: the western sub-regions of the basin, where forest-to-agriculture conversion is concentrated and pixel-level runoff increases are largest, emerge as priority target zones for afforestation and soil conservation measures.

Baseflow and Soil Moisture

With mean annual baseflow rising from 190.33 mm/yr (S1) to 199.11 mm/yr (S4), a total increase of 8.78 mm (4.61%), the result shows an intrinsic response in subsurface hydrology (Tables 7 & 8). In the VIC model framework, baseflow originates from the third soil layer and serves as a direct proxy for groundwater recharge and deep-soil drainage. S1 to S4, the long-term mean of layer 1 soil moisture changed by only about 0.02 mm. This is within the model closure and is treated here as a stability check, not as a hydrological result. The reduced evapotranspiration was passed almost entirely into runoff and baseflow rather than into the storage, so soil water storage changed very little. The baseflow gain likely has two causes. First, lower transpiration leaves more water for deep drainage. Second, the change from forest to shrubland may open near-surface pore space and allow more water to percolate into deeper layers (Kayitesi et al., 2022), thereby making more water available for deeper infiltration and baseflow generation.

The rise in baseflow reflects the long-standing debate on how forest loss affects low flows. Two effects pull in opposite directions: lower evapotranspiration leaves more water for recharge and tends to raise baseflow, while reduced infiltration after forest loss tends to lower recharge (Bruijnzeel, 2004; Ogden et al., 2013). In this basin, the evapotranspiration effect dominates, so baseflow increases. The result should be read with care, because VIC baseflow comes from a conceptual lower zone store rather than an explicit groundwater model (Liang et al., 1994b), so it indicates direction and approximate size rather than an exact groundwater response.

Evapotranspiration

As shown in Tables 7 & 8, the mean annual ET steadily decreases from 929.35 mm/yr (S1) to 913.47 mm/yr (S4), accounting for a total decrease of 15.88 mm (1.71%). ET rates are often higher in forests with deep roots and dense canopies (O'Connor et al., 2021). The main cause of the decrease in ET is the loss of forest cover (a 13.02% reduction in forest area). Deforestation also decreased the canopy interception, which results in a weakened regional water cycle and a drop in atmospheric moisture. Although LULC was identified as the main driver by our modelling approach, which helps reduce evaporative losses from the surface, it is important to recognise that increased irrigation efficiency within the basin may serve as a confounding factor (Chen et al., 2018). In this regard, irrigation abstraction from subsurface layers was not dynamically configured in the VIC model runs; irrigation was held constant and not explicitly represented, so the simulated scenario differences reflect land-cover change alone rather than changes in irrigation practice. The potential feedback loops resulting from the loss of evaporative cooling include increased Land Surface Temperature (LST) and Urban Heat Island (UHI) effects (Zhao et al., 2025).

Table 7: Comparative study of hydrological variables across four LULC scenarios (Mean ET, Surface Runoff, Baseflow and Soil Moisture)

Hydrological Parameters	S1 (LULC-1985)	S2 (LULC-1995)	S3 (LULC-2005)	S4 (LULC-2015)
Surface Runoff	351.27	352.28	353.94	358.44
Evapotranspiration	929.35	927.06	923.27	913.47
Baseflow	190.33	191.65	193.78	199.11
Soil Moisture(L1)	198.62	198.13	198.45	198.60

Table 8: Net Hydrological Changes (S4 vs S1)

Hydrological Parameters	S1Value (LULC-1985)	S4 Value (LULC-2015)	Net Change (S4-S1)	% of Change
Surface Runoff	351.27 mm	358.44 mm	+7.17 mm Increase	+2.04%
Evapotranspiration	929.35 mm	913.47 mm	-15.88 mm Decrease	-1.71 %
Baseflow	190.33 mm	199.11 mm	+8.78 mm Increase	+4.61 %
Soil Moisture (L1)	198.62 mm	198.60 mm	-0.02 mm Decrease	-0.01%

The fall in evapotranspiration follows from the physiological contrast between forest and the cover that replaced it. Forests transpire more than crops and shrubs because of their deeper roots, larger leaf area, higher canopy conductance, and rougher canopy, which together sustain water vapour exchange (Zhang et al., 2001; Bonan, 2008). As the forest gives way to agriculture, both transpiration and canopy interception decline, reducing basin evapotranspiration and leaving more water to be split between runoff and baseflow.

However, this surplus anomaly in water availability is precarious; it heavily relies on suppressed ET, making the subsurface hydrological system potentially less resilient to future climatic warming that could increase evaporative demand (Tan et al., 2021).

This table summarises the increase or decrease in the mean hydrological parameters solely due to the LULC change between 1985 (S1) and 2015 (S4) while holding the climate constant. Tables 5 and 6 show that the basin stays strongly ET dominated ET-dominated across all four scenarios, with ET near 930 to 913 mm per year against runoff near 350 to 360 mm and baseflow near 190 to 200 mm. The land use change moves about 16 mm per year out of ET and into runoff (about 7 mm) and baseflow (about 9 mm). The change is therefore less about the total water balance and more about how water is partitioned, with a shift towards faster pathways that carry more sediment in the wet season and a modest baseflow gain that slightly supports dry season flow.

Subdued Basin Scale Response and Counterbalancing Effect on Runoff

A notable feature of this study, in line with the well-known scale dependence of land-use hydrology, is the subdued basin-scale response: despite a substantial forest loss of about 1880 km^2, basin-wide hydrological changes (e.g., a 7 mm rise in runoff) remain moderate. A detailed pixel-level analysis showed that this apparently subdued response is explained by a counterbalancing effect playing out across the basin. The current analysis shows that around 2143.71 km² of the basin experiences LULC changes that reduce surface runoff, such as shifts toward less erosion-prone or more water-retentive cover. At the same time, 848.57 km² experienced changes that increased runoff response. This indicated that a substantial land transition occurs in the opposite direction within the different sub-regions of the basin, creating a self-cancelling net effect at the larger basin scale. This finding is critical for water resources management, emphasising that localised impacts, such as flood risk, may be severe even when aggregate basin statistics appear moderate.

This pattern is an example of the scale dependence that is well documented in distributed hydrology. Land-use change of opposite nature in different parts of a basin partly cancels at the outlet, weakening the aggregate signal (Andreassian 2004). The contribution here is not the existence of the effect, but its mapping for the Tel basin, which shows where runoff increases and where it decreases. This matters for management because flood and erosion risks can increase sharply in sub-areas that shift towards higher runoff, even when the basin average looks moderate, thereby increasing sediment mobilisation risks. The identification of the counterbalancing effect is essential here, as it explains how and why large-scale deforestation did not always produce a corresponding extreme aggregate hydrological response.

The validated VIC model results confirm that anthropogenic LULC changes are destabilising the Tel River basin's hydrological balance, shifting it towards a regime characterised by lower evaporative cooling, higher flood risk, and altered recharge patterns.

This study successfully isolated the impacts of LULC by holding climatic variables constant throughout the study period. Future studies should integrate climatic variables to examine the combined effect of LULC and climate change, thereby improving understanding of their interdependencies. Integrative studies are more valuable and crucial for providing actionable insights to planners and policymakers who seek sustainable water resources management (IWRM) and aim to mitigate the negative consequences of ongoing land use and land change on hydrological resources.

4. Conclusion

This comprehensive study utilised the VIC model, a sophisticated physically based distributed hydrological model, to assess the long-term impacts of LULCC on the hydrological regime of the Tel River basin.

The Tel River basin has experienced significant LULC changes over the 30-year study period: a 13.02% decrease in forested area, most of it converted to agriculture, and an

increase in built-up area from a small base. These changes caused some measurable disturbances in the basin's water balance, with a 2.04% increase in surface runoff, a 1.71% reduction in evapotranspiration, and a 4.61% increase in baseflow, while long-term soil water storage stayed essentially unchanged. The overall decrease in ET, coupled with the rise in runoff and baseflow, indicates a shift towards a more reactive hydrological regime, reducing ET-driven water recycling and increasing sediment mobilisation risks.

Pixel-level analysis further showed that opposing land use transitions in different sub-regions partly cancel at the basin outlet, so the moderate basin-average response conceals locally severe increases in flood and erosion risk. Taken together, the results indicate that anthropogenic LULCC is shifting the basin towards a regime of lower evaporative recycling, faster runoff pathways, and altered recharge, and that management attention should focus on the sub-regions where runoff is increasing, particularly in the western part of the basin. Because the climatic forcing was held constant, these changes are attributable solely to land-use change. Future studies should couple transient climate forcing with LULC scenarios, and represent irrigation dynamically, to provide actionable insight for planners pursuing integrated water resources management (IWRM) in the basin.

This study successfully isolated the impacts of LULC by holding climatic variables constant throughout the study period. Future studies should integrate climatic variables to examine the combined effect of LULC and climate change, thereby improving understanding of their interdependencies. Integrative studies are crucial for providing actionable insights to planners and policymakers seeking sustainable water resource management (IWRM) and aiming to mitigate the negative consequences of ongoing land use and land change on hydrological resources.

References

Abdulla Fayez, A., D. P. Lettenmaier, E. F. Wood, and S. J. A. 1996. “Application of a Macroscale Hydrologic Model to Estimate the Water Balance of Catchments across Southeast Australia.” 101(D3):7449–7459.

ASCE. 1993. “Criteria for Evaluation of Watershed Models” by the ASCE Task Committee on Definition of Criteria for Evaluation of Watershed Models of the Watershed Management Committee, Irrigation and Drainage Division. 119(3):429–442. https://doi.org/10.1061/(ASCE)0733-9437(1993)119:3(429)

Behera, M. D., P. Tripathi, P. Das, S. K. Srivastava, P. S. Roy, C. Joshi, P. R. Behera, J. Deka, P. Kumar, M. L. Khan, O. P. Tripathi, T. Dash, and Y. V. N. Krishnamurthy. 2018. “Remote Sensing Based Deforestation Analysis in Mahanadi and Brahmaputra River Basin in India since 1985.” *Journal of Environmental Management* 206:1192–1203. https://doi.org/10.1016/j.jenvman.2017.10.015

Berihun, M. L., A. Tsunekawa, N. Haregeweyn, D. T. Meshesha, E. Adgo, M. Tsubo, T. Masunaga, A. A. Fenta, D. Sultan, M. Yibeltal, and K. Ebabu. 2019. “Hydrological Responses to Land Use/Land Cover Change and Climate Variability in Contrasting Agro-Ecological Environments of the Upper Blue Nile Basin, Ethiopia.” *Science of the Total Environment* 689:347–365. https://doi.org/10.1016/j.scitotenv.2019.06.338

Bonan, G. B. 2008. “Forests and Climate Change: Forcings, Feedbacks, and the Climate Benefits of Forests.” *Science* 320(5882):1444–1449. https://doi.org/10.1126/science.1155121

Bosch, J. M., and J. D. Hewlett. 1982. “A Review of Catchment Experiments to Determine the Effect of Vegetation Changes on Water Yield and Evapotranspiration.” *Journal of Hydrology* 55(1–4):3–23. https://doi.org/10.1016/0022-1694(82)90117-2

Breiman, L. 2001. “Random Forests.” *Machine Learning* 45(1):5–32. https://doi.org/10.1023/A:1010933404324

Bruijnzeel, L. A. 2004. “Hydrological Functions of Tropical Forests: Not Seeing the Soil for the Trees.” 104. https://doi.org/10.1016/j.agee.2004.01.015

Chen, Y., J. Niu, S. Kang, and X. Zhang. 2018. “Effects of Irrigation on Water and Energy Balances in the Heihe River Basin Using VIC Model under Different Irrigation Scenarios.” *Science of the Total Environment* 645:1183–1193. https://doi.org/10.1016/j.scitotenv.2018.07.254

Cherkauer, K. A., L. C. Bowling, and D. P. Lettenmaier. 2003. “Variable Infiltration Capacity Cold Land Process Model Updates.” *Global and Planetary Change* 38(1):151–159. https://doi.org/10.1016/S0921-8181(03)00025-0

Connor, J. C. O., S. C. Dekker, A. Staal, O. A. Tuinenburg, K. T. Rebel, and M. J. Santos. 2021. “Forests Buffer against Variations in Precipitation.” 4686–4696. https://doi.org/10.1111/gcb.15763

Cortes, C., and V. Vapnik. 1995. “Support-Vector Networks.” *Machine Learning* 20(3):273–297. https://doi.org/10.1007/BF00994018

Cosby, B. J., G. M. Hornberger, R. B. Clapp, and T. R. Ginn. 1984. “A Statistical Exploration of the Relationships of Soil Moisture Characteristics to the Physical Properties of Soils.” *Water Resources Research* 20(6):682–690. https://doi.org/10.1029/WR020i006p00682

Crompton, O. 2019. “Emulation of the Saint Venant Equations Enables Rapid and Accurate Predictions of Infiltration and Overland Flow Velocity on Spatially Heterogeneous Surfaces.” https://doi.org/10.1029/2019WR025146

Dadhwal, V. K., S. P. Aggarwal, and N. Mishra. 2010. “Hydrological Simulation of Mahanadi River Basin and Impact of Land Use/Land Cover Change on Surface Runoff Using a Macro Scale Hydrological Model.”

Farr, T., P. Rosen, E. Caro, R. Crippen, R. Duren, S. Hensley, M. Kobrick, M. Paller, E. Rodriguez, L. Roth, D. Seal, S. Shaffer, J. Shimada, J. Umland, M. Werner, M. Oskin, D. Burbank, and D. Alsdorf. 2007. “The Shuttle Radar Topography Mission.” *Reviews of Geophysics* 45. https://doi.org/10.1029/2005RG000183

Franchini, M., and M. Pacciani. 1991. "Comparative Analysis of Several Conceptual Rainfall-Runoff Models." *Journal of Hydrology* 122(1):161–219. https://doi.org/10.1016/0022-1694(91)90178-K

Garg, V., S. P. Aggarwal, P. K. Gupta, B. R. Nikam, P. K. Thakur, S. K. Srivastav, and A. Senthil Kumar. 2017. "Assessment of Land Use Land Cover Change Impact on Hydrological Regime of a Basin." *Environmental Earth Sciences* 76(18):635. https://doi.org/10.1007/s12665-017-6976-z

Garg, V., B. R. Nikam, P. K. Thakur, S. P. Aggarwal, P. K. Gupta, and S. K. Srivastav. 2019. "Human-Induced Land Use Land Cover Change and Its Impact on Hydrology." *HydroResearch* 1:48–56. https://doi.org/10.1016/j.hydres.2019.06.001

Gashaw, T., T. Tulu, M. Argaw, and A. W. Worqlul. 2018. "Modeling the Hydrological Impacts of Land Use/Land Cover Changes in the Andassa Watershed, Blue Nile Basin, Ethiopia." *Science of the Total Environment* 619–620:1394–1408. https://doi.org/10.1016/j.scitotenv.2017.11.191

Ghimire, U., S. Shrestha, S. Neupane, S. Mohanasundaram, and O. Lorphensri. 2021. "Climate and Land-Use Change Impacts on Spatiotemporal Variations in Groundwater Recharge: A Case Study of the Bangkok Area, Thailand." *Science of the Total Environment* 792:148370. https://doi.org/10.1016/j.scitotenv.2021.148370

Guru, N., and R. Jha. 2015. "Flood Frequency Analysis of Tel Basin of Mahanadi River System, India Using Annual Maximum and POT Flood Data." *Aquatic Procedia* 4:427–434. https://doi.org/10.1016/j.aqpro.2015.02.057

Hengade, N., and T. I. Eldho. 2019. "Relative Impact of Recent Climate and Land Cover Changes in the Godavari River Basin, India." *Journal of Earth System Science* 128(4):94. https://doi.org/10.1007/s12040-019-1135-4

Kayitesi, N. M., A. C. Guzha, and G. Mariethoz. 2022. "Impacts of Land Use Land Cover Change and Climate Change on River Hydro-Morphology—A Review of Research Studies in Tropical Regions." *Journal of Hydrology* 615(PA):128702. https://doi.org/10.1016/j.jhydrol.2022.128702

Kumari, N., A. Srivastava, B. Sahoo, N. S. Raghuwanshi, and D. Bretreger. 2021. "Identification of Suitable Hydrological Models for Streamflow Assessment in the Kangsabati River Basin, India, by Using Different Model Selection Scores." *Natural Resources Research* 30(6):4187–4205. https://doi.org/10.1007/s11053-021-09919-0

Liang, X., D. P. Lettenmaier, E. F. Wood, and S. J. Burges. 1994a. "A Simple Hydrologically Based Model of Land Surface Water and Energy Fluxes for General Circulation Models." *Journal of Geophysical Research: Atmospheres* 99(D7):14415–14428. https://doi.org/10.1029/94JD00483

Liang, X., D. P. Lettenmaier, E. F. Wood, and S. J. Burges. 1994b. "A Simple Hydrologically Based Model of Land Surface Water and Energy Fluxes for General Circulation Models." *Journal of Geophysical Research* 99(D7). https://doi.org/10.1029/94JD00483

Liang, X., D. P. Lettenmaier, and E. F. Wood. 1996. "One-Dimensional Statistical Dynamic Representation of Subgrid Spatial Variability of Precipitation in the Two-Layer Variable Infiltration Capacity Model." 101(1):403–4022.

Lohmann, D., R. Nolte-Holube, and E. Raschke. 1996. "A Large-Scale Horizontal Routing Model to Be Coupled to Land Surface Parametrization Schemes." *Tellus, Series A: Dynamic Meteorology and Oceanography* 48(5):708–721. https://doi.org/10.3402/tellusa.v48i5.12200

Mishra, S. S., and R. Nagarajan. 2011. "Spatio-Temporal Drought Assessment in Tel River Basin Using Standardized Precipitation Index (SPI) and GIS." *Geomatics, Natural Hazards and Risk* 2(1):79–93. https://doi.org/10.1080/19475705.2010.533703

Moriasi, D. N., J. G. Arnold, M. W. Van Liew, R. L. Bingner, R. D. Harmel, and T. L. Veith. 2007. "Model Evaluation Guidelines for Systematic Quantification of Accuracy in Watershed Simulations." 50(3):885–900.

Muñoz-Sabater, J., E. Dutra, A. Agustí-Panareda, C. Albergel, G. Arduini, G. Balsamo, S. Boussetta, M. Choulga, S. Harrigan, H. Hersbach, B. Martens, D. G. Miralles, M. Piles, N. J. Rodríguez-Fernández, E. Zsoter, C. Buontempo, and J.-N. Thépaut. 2021. "ERA5-Land: A State-of-the-Art Global Reanalysis Dataset for Land Applications." *Earth System Science Data*. https://doi.org/10.5194/essd-2021-82

Nachtergaele, F., H. Van Velthuizen, D. Wiberg, and M. Henry. 2023. *Harmonized World Soil Database Version 2.0*. https://doi.org/10.4060/cc3823en

Naha, S., M. A. Rico-Ramirez, and R. Rosolem. 2021. "Quantifying the Impacts of Land Cover Change on Hydrological Responses in the Mahanadi River Basin in India." *Hydrology and Earth System Sciences* 25(12):6339–6357. https://doi.org/10.5194/hess-25-6339-2021

Niemeyer, R. J., Y. Cheng, Y. Mao, J. R. Yearsley, and B. Nijssen. 2018. "A Thermally Stratified Reservoir Module for Large-Scale Distributed Stream Temperature Models with Application in the Tennessee River Basin." *Water Resources Research* 54(10):8103–8119. https://doi.org/10.1029/2018WR022615

Nikam, B. R., V. Garg, K. Jeyaprakash, P. K. Gupta, S. K. Srivastav, P. K. Thakur, and S. P. Aggarwal. 2018. "Analyzing Future Water Availability and Hydrological Extremes in the Krishna Basin under Changing Climatic Conditions." *Arabian Journal of Geosciences* 11(19):581. https://doi.org/10.1007/s12517-018-3936-1

Ogden, F. L., T. D. Crouch, R. F. Stallard, and J. S. Hall. 2013. "Effect of Land Cover and Use on Dry Season River Runoff, Runoff Efficiency, and Peak Storm Runoff in the Seasonal Tropics of Central Panama." 49:8443–8462. https://doi.org/10.1002/2013WR013956

Patidar, N., and M. D. Behera. 2019. "How Significantly Do Land Use and Land Cover (LULC) Changes Influence

the Water Balance of a River Basin? A Study in Ganga River Basin, India." *Proceedings of the National Academy of Sciences, India Section A: Physical Sciences* 89(2):353–365. https://doi.org/10.1007/s40010-017-0426-x

Quinlan, J. R. 1986. "Induction of Decision Trees." *Machine Learning* 1(1):81–106. https://doi.org/10.1007/BF00116251

Reynolds, C. A., T. J. Jackson, and W. J. Rawls. "Estimating Soil Water-Holding Capacities by Linking the Food and Agriculture…" [Reference incomplete in the supplied source.]

Roy, P., A. Roy, P. Joshi, M. Kale, V. Srivastava, S. Srivastava, R. Dwevidi, C. Joshi, M. Behera, P. Meiyappan, Y. Sharma, A. Jain, J. Singh, Y. Palchowdhuri, R. Ramachandran, B. Pinjarla, V. Chakravarthi, N. Babu, M. Gowsalya, … D. Kushwaha. 2015. "Development of Decadal (1985–1995–2005) Land Use and Land Cover Database for India." *Remote Sensing* 7(3):2401–2430. https://doi.org/10.3390/rs70302401

Shrestha, R. R., M. A. Schnorbus, A. T. Werner, and A. J. Berland. 2012. "Modelling Spatial and Temporal Variability of Hydrologic Impacts of Climate Change in the Fraser River Basin, British Columbia, Canada." *Hydrological Processes* 26(12):1840–1860. https://doi.org/10.1002/hyp.9283

Sulamo, M. A., A. K. Kassa, and N. T. Roba. 2021. "Evaluation of the Impacts of Land Use/Cover Changes on Water Balance of Bilate Watershed, Rift Valley Basin, Ethiopia." *Water Practice and Technology* 16(4):1108–1127. https://doi.org/10.2166/wpt.2021.063

Tan, S., H. Wang, I. C. Prentice, and K. Yang. 2021. "Land-Surface Evapotranspiration Derived from a First-Principles Primary Production Model." [Publication details incomplete in the supplied source.]

Tavakoly, A. A., A. D. Snow, C. H. David, M. L. Follum, D. R. Maidment, and Z.-L. Yang. 2017. "Continental-Scale River Flow Modeling of the Mississippi River Basin Using High-Resolution NHDPlus Dataset." *Journal of the American Water Resources Association* 53(2):258–279. https://doi.org/10.1111/1752-1688.12456

Verma, N., R. K. Patel, and P. Choudhari. 2022. "Watershed Prioritization for Soil Conservation in a Drought-Prone Watershed of Eastern India: Tel River Basin, Odisha." *Geology, Ecology, and Landscapes*:1–14. https://doi.org/10.1080/24749508.2021.2022830

Zamani Sabzi, H., H. A. Moreno, R. Fovargue, X. Xue, Y. Hong, and T. M. Neeson. 2019. "Comparison of Projected Water Availability and Demand Reveals Future Hotspots of Water Stress in the Red River Basin, USA." *Journal of Hydrology: Regional Studies* 26:100638. https://doi.org/10.1016/j.ejrh.2019.100638

Zhang, L., W. R. Dawes, and G. R. Walker. 2001. "Response of Mean Annual Evapotranspiration to Vegetation Changes at Catchment Scale." 37(3):701–708.

Zhao, L., X. Fan, and T. Hong. 2025. "Urban Heat Island Effect: Remote Sensing Monitoring and Assessment—Methods, Applications, and Future Directions." 1–55.

Zhao, R.-J. 1980. "The Xinanjiang Model." *Proceedings of the Oxford Symposium*.